INTERNATIONAL JOURNAL FOR NUMERICAL METHODS IN FLUIDS, VOL. 9, 1413–1426 (1989)

NUMERICAL SIMULATION OF AN IMPINGING JET ON A FLAT PLATE

SHU-HAO CHUANG

Department of Mechanical Engineering, National Chung-Hsing University, Taichung, Taiwan 40227, R.O.C.

SUMMARY

Two-dimensional normal impinging jet flowfields, with or without an upper plate, were analysed by employing an implicit bidiagonal numerical method developed by Lavante and Thompkins Jr. The Jones–Launder K–ε two-equation turbulent model was employed to study the turbulent effects of the impinging jet flowfield. The upper plate surface pressure, the ground plane pressure and other physical parameters of the momentum flowfield were calculated at various jet exit height and jet inlet Reynolds numbers. These results were compared with those of Beam and Warming's numerical method, Hsiao and Chuang, and others, along with experimental data. The potential core length of the impinging jet without an upper plate is longer than that of the free jet because of the effects of the ground plane, while the potential core length of the impinging jet with an upper plate is shorter than that of the free jet because of the effects of the upper plate. This phenomenon in the present analysis provides a fundamental numerical study of an impinging jet and a basis for further analysis of impinging jet flowfields on a variable angle plate.

KEY WORDS Impinging jet MacCormack implicit scheme Implicit bidiagonal numerical method

INTRODUCTION

Analysis of the impinging jet is very important because of its wide application to engineering problems such as the take-off of VTOL aircraft and the vectoring of fighter planes. Studies of a single impinging plane jet may provide some basic understanding of multiple impinging jets. The ground plane effect in impinging jet flowfields is important to the performance of VTOL aircraft design. The vectored jet impinging on the ground plane and the wall jet flowfield developed along the downstream ground plane are very complicated phenomena. To approach these phenomena by theoretical analysis or experimental measurement can be quite difficult. The cost of experimentation may be substantial in order to understand the structure of impinging jet flowfields. Therefore numerical simulation may be a cost-effective approach to the study of impinging jet flowfields. Two-dimensional impinging jet flowfields can be divided into three regions—(1) the free jet region, (2) the impingement region and (3) the wall jet region—as shown in Figure 1.

Theoretical analysis of such flows has been concerned with either solving the full Navier–Stokes equations[1–4] or finding solutions for several separate regions.[5,6] Two- and three-dimensional impinging jet flowfields were studied by Bower *et al.*,[7] who utilized the stream function–vorticity and Jones–Launder K–ε turbulent two-equation model. These results show good agreement between predictions and experimental data. Incompressible, inviscid, rotational impingement problems have also been considered.[8] The predicted ground plane pressure distributions, centreline velocity decay and oblique impingement flowfield structure of normal axisymmetric

0271–2091/89/111413–14$07.00
© 1989 by John Wiley & Sons, Ltd.
Received September 1988
Revised January 1989

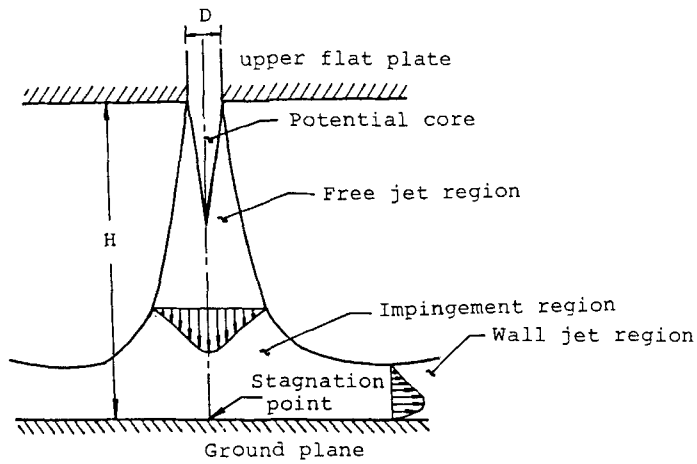

Figure 1. Schematic of the impinging jet

impingement and oblique impingement two-dimensional jets compared well with observations. This study indicates that the impingement region is dominated by a balance of the pressure forces due to flow deflection and the inertial forces of convection. Hence the inviscid rotational flow model for calculating the impingement region is a reasonable assumption. Agarwal and Bower[9] used the same turbulence model to predict the impinging jet flowfield, with an upper plate, at various Reynolds numbers and exit heights.

However, these investigations were limited to the use of streamfunction–vorticity for solving the Navier–Stokes equations. Insight into the impinging jet flowfield is needed to use the primitive variables directly for solving the finite difference governing equations. In viscous flow the fine mesh spacing makes the MacCormack scheme with the explicit method[10, 11] extremely costly. Implicit methods[12, 13] make the use of large time steps possible but require the inversion of block tridiagonal matrices. Impinging jet flowfield analysis by the Beam and Warming method has been performed by Hwang and Liu.[14] A method recently developed by MacCormack[15] has eliminated this disadvantage by introducing a predictor–corrector scheme that only requires the inversion of block bidiagonal matrices. The resulting finite difference equations are either upper or lower block bidiagonal equations that can be easily solved in one sweep. Unfortunately, this method was demonstrated only for a simple case .The intention here is to provide a simple implicit method to solve two-dimensional, viscous, compressible impinging jet flowfields. Recently an implicit bidiagonal numerical method, which is very similar to the new MacCormack method, was developed by Lavante and Thompkins Jr.[16] This method has some advantages, namely the programming structure is simple and no matrix inversion is necessary. The resulting matrices are block bidiagonal and can be easily solved. The calculations presented were performed by using the implicit bidiagonal numerical method for solving the impinging jet, without or with an upper plate, at various jet inlet Reynolds numbers and jet exit heights.

GOVERNING EQUATIONS

In order to simplify the impinging jet problem, the following assumptions are made:

1. The flowfield is a single normal impingement two-dimensional jet.
2. Both ground plane and upper plate surface are adiabatic.

3. The fluid is an ideal gas with constant specific heat.
4. Gravitational effects are not considered.
5. Crossflow is not coupled with jet flow.

The two-dimensional compressible Navier–Stokes equations can be written in conservation form[17] as

$$\frac{\partial \mathbf{U}}{\partial t}+\frac{\partial \mathbf{F}(\mathbf{U})}{\partial x}+\frac{\partial \mathbf{G}(\mathbf{U})}{\partial y}=\mathbf{0}, \tag{1}$$

where

$$\mathbf{U}=\begin{bmatrix}\rho\\ \rho u\\ \rho v\\ e\end{bmatrix},\qquad \mathbf{F}=\begin{bmatrix}\rho u\\ \rho u^2+\sigma_x\\ \rho uv+\tau_{xy}\\ (e+\sigma_x)u+\tau_{xy}v-k\dfrac{\partial T}{\partial x}\end{bmatrix},\qquad \mathbf{G}=\begin{bmatrix}\rho v\\ \rho uv+\tau_{xy}\\ \rho v^2+\sigma_y\\ (e+\sigma_y)v+\tau_{xy}u-k\dfrac{\partial T}{\partial y}\end{bmatrix},$$

with

$$P=(\gamma-1)[e-\tfrac{1}{2}\rho(u^2+v^2)],$$

$$\sigma_x=P-\lambda\left(\frac{\partial u}{\partial x}+\frac{\partial v}{\partial y}\right)-2\mu\frac{\partial u}{\partial x},$$

$$\tau_{xy}=-\mu\left(\frac{\partial u}{\partial y}+\frac{\partial v}{\partial x}\right),$$

$$\sigma_y=P-\lambda\left(\frac{\partial u}{\partial x}+\frac{\partial v}{\partial y}\right)-2\mu\frac{\partial v}{\partial y}.$$

Equation (1) can be expressed in dimensionless form by defining dimensionless variables[16]

$$\rho'=\rho/\rho_{\text{jet}},\qquad x'=x/D,\qquad y'=y/D,$$

$$u'=u/a_{\text{jet}},\qquad v'=v/a_{\text{jet}},\qquad T'=T/T_{\text{jet}},$$

$$P'=P/\rho_{\text{jet}}a_{\text{jet}}^2,\qquad e'=e/\rho_{\text{jet}}a_{\text{jet}}^2,\qquad \mu'=\mu/\mu_{\text{jet}},$$

$$k'=k/k_{\text{jet}},\qquad t'=t(a_{\text{jet}}/D),\qquad R_{e_0}=\rho_{\text{jet}}a_{\text{jet}}D/\mu_{\text{jet}},$$

$$Pr=\mu_{\text{jet}}C_P/k_{\text{jet}}.$$

The dimensionless form of equation (1) is

$$\frac{\partial \mathbf{U}'}{\partial t'}+\frac{\partial \mathbf{F}'(\mathbf{U}')}{\partial x'}+\frac{\partial \mathbf{G}'(\mathbf{U}')}{\partial y'}=\mathbf{0}, \tag{2}$$

where

$$\mathbf{U}'=\begin{bmatrix}\rho'\\ \rho'u'\\ \rho'v'\\ e'\end{bmatrix},$$

$$\mathbf{F}'=\begin{bmatrix}\rho' u' \\ \rho' u'^2+\sigma_x' \\ \rho' u' v'+\tau_{xy}' \\ (e'+\sigma_x')u'+\tau_{xy}' v'-k'\dfrac{1}{Pr\,Re_0\,(\gamma-1)}\dfrac{\partial T'}{\partial x'}\end{bmatrix},$$

$$\mathbf{G}'=\begin{bmatrix}\rho' v' \\ \rho' u' v'+\tau_{xy}' \\ \rho' v'^2+\sigma_y' \\ (e'+\sigma_y')v'+\tau_{xy}' u'-k'\dfrac{1}{Pr\,Re_0(\gamma-1)}\dfrac{\partial T'}{\partial y'}\end{bmatrix},$$

with

$$P'=(\gamma-1)[e'-\tfrac{1}{2}\rho'(u'^2+v'^2)],$$

$$\sigma_x'=P'-\frac{\lambda'}{Re_0}\left(\frac{\partial u'}{\partial x'}+\frac{\partial v'}{\partial y'}\right)-2\frac{\mu'}{Re_0}\frac{\partial u'}{\partial x'},$$

$$\tau_{xy}'=-\frac{\mu'}{Re_0}\left(\frac{\partial u'}{\partial y'}+\frac{\partial v'}{\partial x'}\right),$$

$$\sigma_y'=P'-\frac{\lambda'}{Re_0}\left(\frac{\partial u'}{\partial x'}+\frac{\partial v'}{\partial y'}\right)-2\frac{\mu'}{Re_0}\frac{\partial v'}{\partial y'}.$$

The primes will be dropped later for convenience. The turbulent governing equations with time average can be expressed in dimensionless conservation form as

$$\frac{\partial \bar{\mathbf{U}}}{\partial t}+\frac{\partial \bar{\mathbf{F}}}{\partial x}+\frac{\partial \bar{\mathbf{G}}}{\partial y}=\mathbf{0}. \tag{3}$$

The eddy viscosity μ_t is evaluated from a modified K–ε model.[14, 18–20] The non-dimensional governing equation for this turbulence model in strong conservation form is

$$\frac{\partial \mathbf{U}_t}{\partial t}+\frac{\partial \mathbf{F}_t}{\partial x}+\frac{\partial \mathbf{G}_t}{\partial y}+\mathbf{H}_t=\mathbf{0}, \tag{4}$$

where

$$\mathbf{U}_t=\begin{bmatrix}\bar{\rho}K \\ \bar{\rho}\varepsilon\end{bmatrix},\qquad \mathbf{F}_t=\begin{bmatrix}\bar{\rho}\bar{u}K-\dfrac{1}{Re_0}\left(\mu_l+\dfrac{\mu_t}{\sigma_K}\right)K_x \\ \bar{\rho}\bar{u}\varepsilon-\dfrac{1}{Re_0}\left(\mu_l+\dfrac{\mu_t}{\sigma_\varepsilon}\right)\varepsilon_x\end{bmatrix},\quad \mathbf{G}_t=\begin{bmatrix}\bar{\rho}\bar{v}K-\dfrac{1}{Re_0}\left(\mu_l+\dfrac{\mu_t}{\sigma_K}\right)K_y \\ \bar{\rho}\bar{v}\varepsilon-\dfrac{1}{Re_0}\left(\mu_l+\dfrac{\mu_t}{\sigma_\varepsilon}\right)\varepsilon_y\end{bmatrix},$$

$$\mathbf{H}_t=\frac{-1}{Re_0}\begin{bmatrix}\mu_t\mathbb{P}-Re_0\bar{\rho}\varepsilon-2\mu_l\left(\dfrac{\partial K}{\partial y}\right)^2 \\ \mu_t C_1\dfrac{\varepsilon}{K}\mathbb{P}-C_2\dfrac{\bar{\rho}\varepsilon^2}{K}Re_0+2\dfrac{\mu_l}{\rho}\dfrac{\mu_t}{Re_0}\left(\dfrac{\partial^2\bar{u}}{\partial y}\right)^2\end{bmatrix},$$

with

$$\mathbb{P}=\left(\frac{\partial\bar{u}}{\partial y}+\frac{\partial\bar{u}}{\partial x}\right)^2+2\left(\frac{\partial\bar{u}}{\partial x}\right)^2+2\left(\frac{\partial\bar{v}}{\partial y}\right)^2,\qquad \mu_t=C_\mu\frac{\bar{\rho}K^2}{\varepsilon}Re_0,$$

$$C_\mu = 0{\cdot}09\{\exp[-2{\cdot}5/(1+Rt/50)]\}, \qquad C_1 = 1{\cdot}44, \qquad C_2 = 1{\cdot}92[1-0{\cdot}3\exp(-R_t^2)],$$

$$Rt = \frac{\bar{\rho}K^2}{\mu_l \varepsilon} Re_0, \qquad \sigma_K = 1{\cdot}0, \qquad \sigma_\varepsilon = 1{\cdot}3.$$

NUMERICAL METHOD

Grid system

The physical region of interest, which is a rectangle in (x, y) co-ordinates, is transformed into a square region in (ξ, η) computational co-ordinates as shown in Figure 2. A suitable transformation that also allows for the packing of grid points in regions of high gradients is:

(1) transverse direction

$$x = w\frac{(\beta'+1)-(\beta'-1)\{[(\beta'+1)/(\beta'-1)]^{1-\xi}\}}{[(\beta'+1)/(\beta'-1)]^{1-\xi}+1}$$

$$\xi = 1 - \frac{\ln\{[\beta'+1-(x/w)]/[\beta'-1+(x/w)]\}}{ln[(\beta'+1)/(\beta'-1)]}; \tag{5}$$

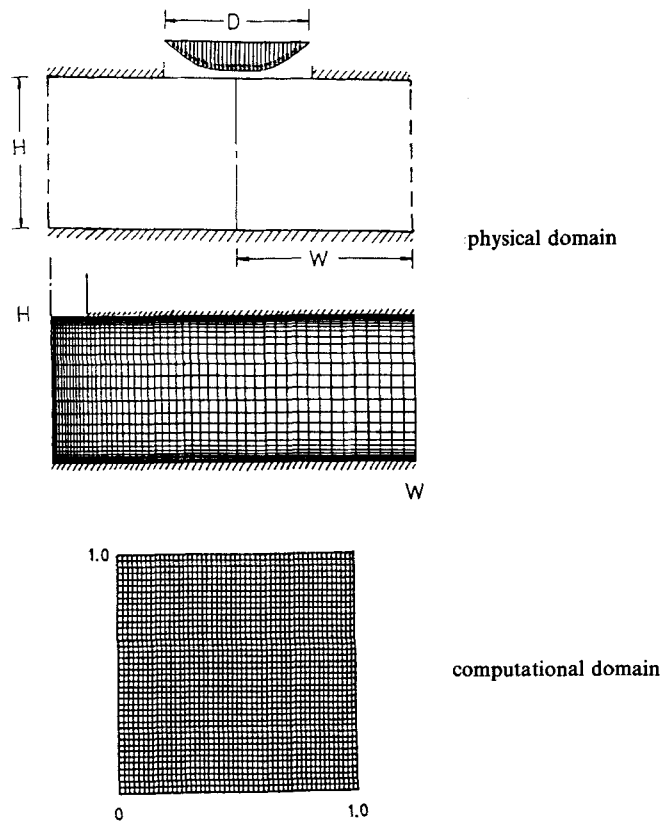

Figure 2. Physical domain and computational domain of the impinging jet

(2) longitudinal direction

$$y=H\frac{(\beta''+1)[(\beta''+1)/(\beta''-1)]^{2\eta-1}-\beta''+1}{2\{1+[(\beta''+1)/(\beta''-1)]^{2\eta-1}\}},$$
$$\eta=\frac{1}{2}+\frac{1}{2}\frac{\ln[(\beta''+2y/H-1)/(\beta''-2y/H+1)]}{\ln[(\beta''+1)/(\beta''-1)]}; \tag{6}$$

where β' and β'' are stretching parameters.

Finite difference equations and numerical solution

In most of the practical calculation cases it is convenient to transform the non-uniform grid system of the physical domain (x, y) into the uniform grid system of the computational domain (ξ, η) as shown in Figure 2. Equation (1) can then be transformed from Cartesian co-ordinates (x, y) into general co-ordinates (ξ, η) as

$$\frac{\partial \hat{\mathbf{U}}}{\partial t}+\frac{\partial \hat{\mathbf{F}}}{\partial \xi}+\frac{\partial \hat{\mathbf{G}}}{\partial \eta}=\mathbf{0}, \tag{7}$$

where

$$\hat{\mathbf{U}}=\mathbf{U}/J, \qquad \hat{\mathbf{F}}=(\mathbf{F}\xi_x+\mathbf{G}\xi_y)/J, \qquad \hat{\mathbf{G}}=(\mathbf{F}\eta_x+\mathbf{G}\eta_y)/J.$$

J is the transformation Jacobian

$$J=\frac{1}{x_\xi y_\eta-x_\eta y_\xi}=\xi_x\eta_y-\xi_y\eta_x. \tag{8}$$

The numerical integration method of equation (7) has been adopted from MacCormack.[15] The resulting integration scheme is explained in detail, in this reference and will therefore not be repeated here. Equation (7) is integrated by the following implicit predictor–corrector set of finite difference equations:

predictor

$$\Delta\hat{\mathbf{U}}^n_{i,j}=-\Delta t\left(\frac{\Delta^+\hat{\mathbf{F}}^n_{i,j}}{\Delta\xi}+\frac{\Delta^+\hat{\mathbf{G}}^n_{i,j}}{\Delta\eta}\right),$$
$$\left(\mathbf{I}-\Delta t\frac{\Delta^+|\hat{\mathbf{A}}|^n}{\Delta\xi}\right)\left(\mathbf{I}-\Delta t\frac{\Delta^+|\hat{\mathbf{B}}|^n}{\Delta\eta}\right)\delta\hat{\mathbf{U}}^{\overline{n+1}}_{i,j}=\Delta\hat{\mathbf{U}}^n_{i,j}, \tag{9}$$
$$\hat{\mathbf{U}}^{\overline{n+1}}_{i,j}=\hat{\mathbf{U}}^n_{i,j}+\delta\hat{\mathbf{U}}^{\overline{n+1}}_{i,j};$$

corrector

$$\Delta\hat{\mathbf{U}}^{n+1}_{i,j}=-\Delta t\left(\frac{\Delta^-\hat{\mathbf{F}}^{\overline{n+1}}_{i,j}}{\Delta\xi}+\frac{\Delta^-\hat{\mathbf{G}}^{\overline{n+1}}_{i,j}}{\Delta\eta}\right),$$
$$\left(\mathbf{I}+\Delta t\frac{\Delta^-|\hat{\mathbf{A}}|^{\overline{n+1}}}{\Delta\xi}\right)\left(\mathbf{I}+\Delta t\frac{\Delta^-|\hat{\mathbf{B}}|^{\overline{n+1}}}{\Delta\eta}\right)\delta\hat{\mathbf{U}}^{n+1}_{i,j}=\Delta\hat{\mathbf{U}}^{n+1}_{i,j}, \tag{10}$$
$$\hat{\mathbf{U}}^{n+1}_{i,j}=\tfrac{1}{2}(\hat{\mathbf{U}}^n_{i,j}+\hat{\mathbf{U}}^{\overline{n+1}}_{i,j}+\delta\hat{\mathbf{U}}^{n+1}_{i,j}).$$

Similarly, equation (4) can be transformed from (x, y) co-ordinates into (ξ, η) co-ordinates and integrated by the MacCormack[15] implicit predictor–corrector set of finite difference equations.

Then the equations for K and ε are solved simultaneously with the other primitive variables. An implicit bidiagonal numerical method[16] was employed to perform the present calculations because it is faster and simpler than existing MacCormack implicit methods. This bidiagonal numerical method does not require the inversion of block tridiagonal matrices. A fourth-order explicit dissipation term[17] is added for each iteration process to help the convergence of the calculations.

Boundary conditions

The initial values of $\Delta t\,|\mathbf{B}|\delta\mathbf{U}$ and $\Delta t\,|\mathbf{A}|\,\delta\mathbf{U}$ must be given for both predictor and corrector steps because a spatial upwind scheme was employed in the present analysis. For simplicity, we denote by $\delta\mathbf{W}$ the expressions that represent the implicit part of the boundary conditions. The boundary conditions in this context can be handled as follows.

(*a*) *At the axisymmetric centre*[16, 21–23]

$$\begin{bmatrix} \rho \\ \rho u \\ \rho v \\ e \end{bmatrix}^{n+1}_{0,i} = \begin{bmatrix} 1 & 0 & 0 & 0 \\ 0 & -1 & 0 & 0 \\ 0 & 0 & 1 & 0 \\ 0 & 0 & 0 & 1 \end{bmatrix} \begin{bmatrix} \rho \\ \rho u \\ \rho v \\ e \end{bmatrix}^{n+1}_{2,j}. \tag{11}$$

(*b*) *At the outlet*[4, 7, 8, 16, 21–23]

$$\begin{bmatrix} \rho \\ \rho u \\ \rho v \end{bmatrix}^{n+1}_{i_{\max},j} = 2\begin{bmatrix} \rho \\ \rho u \\ \rho v \end{bmatrix}^{n+1}_{i_{\max}-1,j} - \begin{bmatrix} \rho \\ \rho u \\ \rho v \end{bmatrix}^{n+1}_{i_{\max}-2,j}, \tag{12}$$

$$T^{n+1}_{i_{\max},j} = P_{i_{\max},j}/[(1/\gamma)\,\rho^{n+1}_{i_{\max},j}], \qquad P^{n+1}_{i_{\max}} = P^{n}_{i_{\max},j}. \tag{13}$$

The same extrapolation was applied to the implicit part of the boundary conditions:

$$\delta\mathbf{W} = 2(|\mathbf{A}|\,\delta\mathbf{U})_{i_{\max}-1} - (|\mathbf{A}|\,\delta\mathbf{U})_{i_{\max}-2} \tag{14}$$

Since, at the time of evaluation of $\delta\mathbf{W}$, the expressions on the LHS of equation (14) are not known, $\delta\mathbf{W}$ will have to be calculated by using an implicit scheme at the three points $i_{\max}$, $i_{\max}-1$ and $i_{\max}-2$.

(*c*) *At the ground plane*

$$u_{i,1} = 0. \qquad v_{i,1} = 0 \qquad \text{(no slip)}, \tag{15}$$

$$\partial T/\partial y = 0 \qquad \text{(adiabatic)}. \tag{16}$$

The corrector value of $\partial\mathbf{W}$ can be obtained by using the same principle from the predictor value of $\Delta t\,|\mathbf{B}|\,\delta\mathbf{U}$ at the point $j=2$.[16]

$$\delta\mathbf{W}^{n+1} = R\,\Delta t(|\mathbf{B}|\,\delta\mathbf{U})^{n+1}_{j=2}, \tag{17}$$

$$(|\mathbf{B}|\,\delta\mathbf{U})^{n+1}_{j=2} = \begin{bmatrix} 0 & 0 & 1 & 0 \\ 0 & 0 & 0 & 0 \\ 0 & 0 & 0 & \gamma-1 \\ 0 & 0 & \gamma e/\rho & 0 \end{bmatrix}^{n+1}_{i,2} \begin{bmatrix} \Delta\rho \\ 0 \\ 0 \\ \Delta e \end{bmatrix}^{n+1}_{i,2} = \begin{bmatrix} 0 \\ 0 \\ (\gamma-1)\Delta e \\ 0 \end{bmatrix}^{n+1}_{i,2}, \tag{18}$$

$$\delta \mathbf{W}^{n+1} = R\,\Delta t(|\mathbf{B}|\,\delta \mathbf{U})_{j=2}^{n+1}$$

$$= \begin{bmatrix} 1 & 0 & 0 & 0 \\ 0 & -1 & 0 & 0 \\ 0 & 0 & -1 & 0 \\ 0 & 0 & 0 & 1 \end{bmatrix} - \Delta t \begin{bmatrix} 0 \\ 0 \\ (\gamma-1)\Delta e \\ 0 \end{bmatrix}_{i-2}^{n+1} = \Delta t \begin{bmatrix} 0 \\ 0 \\ (1-\gamma)\Delta e \\ 0 \end{bmatrix}_{i-2}^{\overline{n+1}}. \quad (19)$$

The predictor value of $\delta \mathbf{W}$ used the following procedure:

$$\delta \mathbf{W}^{\overline{n+1}} = R\,\Delta t(|\mathbf{B}|\delta \mathbf{U})_{j=2}^{n} = \delta \mathbf{W}^{n}. \quad (20)$$

The ground plane may also be placed at the first grid node and the condition $\delta \mathbf{W} = \mathbf{0}$ used.

(*d*) *At the jet inlet and upper plate surface.* The inlet boundary conditions of $u_{1,j}^{n+1}$, $v_{1,j}^{n+1}$ and $T_{1,j}^{n+1}$ of the jet are given in the Reference 22, and

$$\rho_{1,j}^{n+1} = P_{1,j}^{n+1}/[(1/\gamma)T_{i,j}^{n+1}], \quad (21)$$

where the pressure is obtained from the following relation:

$$P_{1,j}^{n+1} = P_{2,j}^{n+1} - \rho_{1,j}^{n+1}\, a_{1,j}^{n}(u_{2,j}^{n+1} - u_{1,j}^{n+1}). \quad (22)$$

The turbulent boundary conditions of K and ε for the upper plate in the computational domain are[4]

$$K = \begin{cases} 0{\cdot}04, & \xi \leqslant 0{\cdot}15, \\ 0{\cdot}02\{1+\sin[3\pi/2 - 5\pi(1-2\xi)]\}, & 0{\cdot}15 \leqslant \xi \leqslant 0{\cdot}5, \\ 0{\cdot}0, & \xi \geqslant 0{\cdot}5, \end{cases} \quad (23)$$

$$\varepsilon = 5K^{3/2}.$$

Both K and ε are assumed to be zero at the ground plane.

RESULTS AND DISCUSSION

The ground plane pressure distribution without an upper plate is shown in Figure 3. The present results show that it is in good agreement with the experimental data of Hsiao and Chuang,[24] Cartwright and Russell[25] and Schauer and Eustis.[26] The centreline velocity decay of the impinging jet without an upper plate is shown in Figure 4. It shows that the present calculation is reasonable when compared with Rubel[8] and Hwang and Liu.[14] The velocity vector diagram of the impinging jet flowfield is shown in Figure 5. The important parameters are the jet inlet Reynolds number and the jet exit height when the impinging jet flowfield has an upper plate. In the present calculation the results can be discussed as follows.

Effects of jet inlet Reynolds number of the impinging flow

In the present analysis we use $Re = 100$ and 1000 to check the effects of the jet inlet Reynolds number on the impinging flow. The jet exit height is $H/D = 2$; $W/D = 4{\cdot}68$, $M = 0{\cdot}1$ and the inlet velocity is as in Reference 9. The ground plane pressure distributions for the two Reynolds numbers are shown in Figure 6. The viscous effects are more important than the convection effects at the ground plane for the smaller Reynolds number ($Re_0 = 100$). Hence a positive pressure gradient is formed when it is along the downstream x-direction and results in a secondary flow in

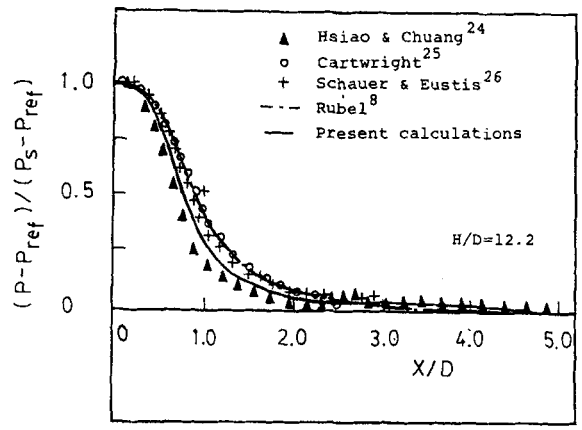

Figure 3. Ground plane pressure distributions of the impinging jet without an upper plate; fully developed jet profile

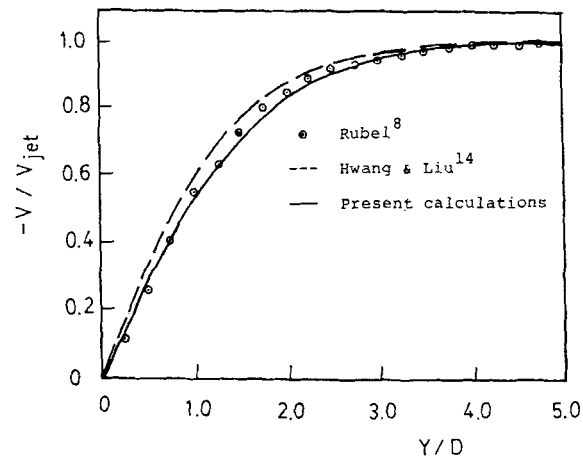

Figure 4. Centreline velocity decay of the impinging jet without an upper plate; fully developed jet profile

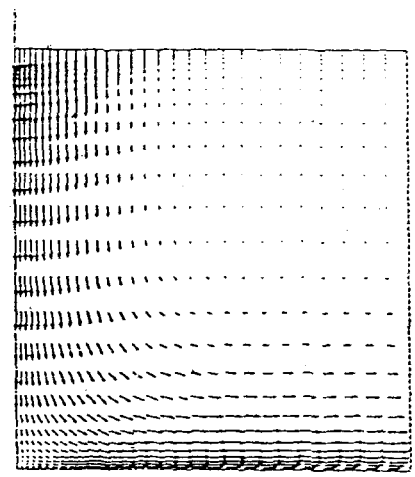

Figure 5. Velocity vector diagram of the impinging jet without an upper plate

the flowfield. The inertial forces of convection are more important than the viscous forces at the higher Reynolds number ($Re_0 = 1000$). Therefore the ground plane pressure value is increased in comparison with the low-Reynolds-number case. The velocity near the upper plate is low for the higher Reynolds number, and the upper plate pressure approaches atmospheric pressure, as shown in Figure 7.

Effects of jet exit height on the impinging flow

The jet exit height is an important parameter in impinging jet flowfields.[8] In the present calculations we take $H/D = 4$, 12 and 20 ($Re_0 = 11\,000$) to analyse the effects of the jet exit height on the impinging flow. The pressure distributions of the ground plane and the upper plate surface for the various jet exit heights are shown in figures 8 and 9 respectively. The pressure in the x-direction approaches atmospheric pressure when $H/D = 4$, as shown in Figure 8. The pressure recovery is quicker when $H/D = 4$ because of fluid acceleration between the ground plane and the upper plate, as shown in Figure 9. The pressure profiles almost coincide with each other when the jet exit height $H/D = 12$ and 20 because the exit height is at or over the transitional region of the free jet. The pressure distributions of the ground plane over the transitional region are almost bell-shaped, as shown in Figure 8. This fact shows that ground plane effects on impinging jet flow with an upper plate can be neglected when the jet exit height is over the transitional region. The centreline

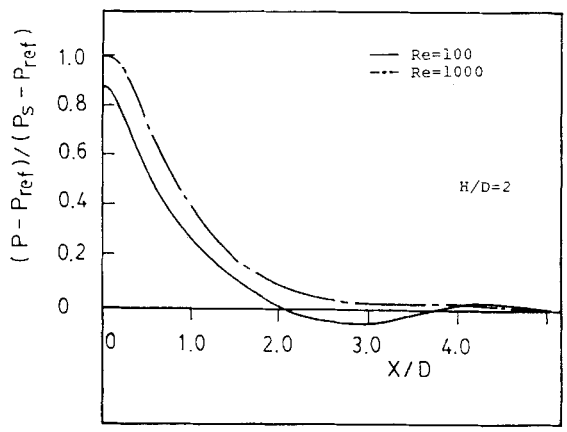

Figure 6. Ground plane pressure distributions of the impinging jet with an upper plate at various Reynolds numbers

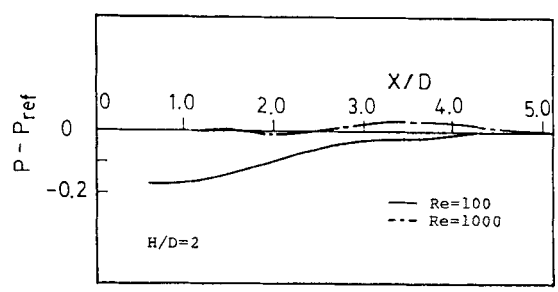

Figure 7. Upper plate surface pressure distributions at various Reynolds numbers

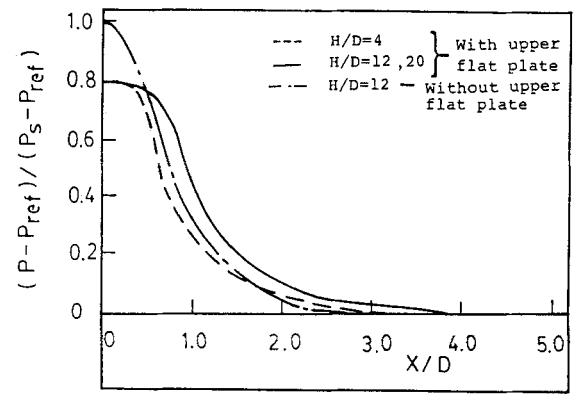

Figure 8. Ground plane pressure distributions of the impinging jet with an upper plate, at various jet exit heights

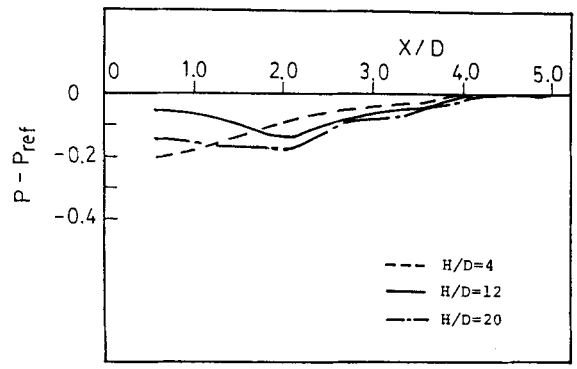

Figure 9. Upper plate surface pressure distributions at various jet heights

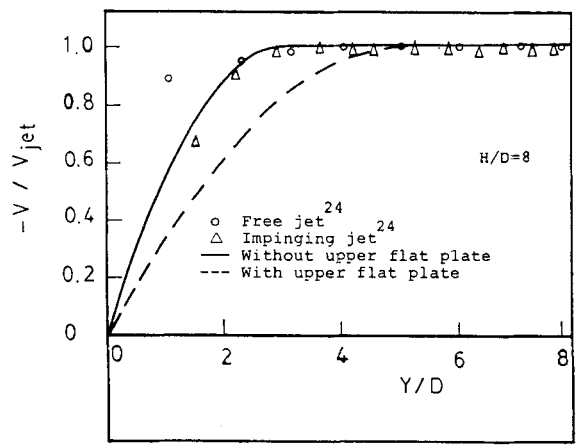

Figure 10. Centreline velocity decay of the free jet and the impinging jet, without and with an upper plate

velocity decay of the free jet and the impinging jet, without and with an upper plate, is shown in Figure 10. The potential core length of the impinging jet without an upper plate ($\approx 5{\cdot}4D$) is longer than that of the free jet ($\approx 4{\cdot}0D$) because the ground plane effects induce a positive pressure gradient. The present centreline velocity decay results of the impinging jet have been compared with the Hsiao and Chuang experimental data[24] and are found to be in good agreement. The potential core length of the impinging jet with an upper plate ($\approx 3{\cdot}2D$) is shorter than that of the free jet ($\approx 4{\cdot}0D$) owing to the effects of the ground plane and upper plate. The upper plate acts as the lower fuselage surface of an aircraft; hence the present analysis can provide a fundamental understanding of V/STOL aircraft designs.

CONCLUDING REMARKS

1. An implicit bidiagonal numerical method[16] has some important advantages, namely the programming structure is simple and no matrix inversion is necessary.
2. The pressure recovery at the ground plane with upper plate flow will be quicker than without upper plate flow.
3. The impinging jet potential core length without an upper plate is longer than that of the free jet owing to the effects of the ground plane. However, the potential core length of the impinging jet with an upper plate is shorter than that of the free jet owing to the effects of the upper plate and ground plane.
4. The positive gradient pressure along the ground plane downstream and the induced secondary flow phenomenon can be eliminated by high-Reynolds-number flow.
5. The pressure distribution of the upper plate can be improved to a partly positive distribution by a high Reynolds number.

ACKNOWLEDGEMENTS

The author wishes to express grateful appreciation to the computer centre of National Chung-Hsing University and to my research assistant Mr. C. S. Wang, and for the suggestions of Dr. F. B. Hsiao.

APPENDIX: NOMENCLATURE

a	sonic velocity
A, B	Jacobian matrices
C_1, C_2, C_μ	coefficients of turbulent model
C_p	specific heat at constant pressure
D	inlet width of the jet
e	total energy per unit volume
F, G	flux vectors
H	jet exit height from ground plane to jet inlet
I	unit matrix
i_{max}, j_{max}	maximum number of grid point in the ξ- and η-direction respectively
K	turbulent kinetic energy
k	thermal conductivity
M	Mach number
P	pressure
Pr	Prandtl number

Re_0	Reynolds number
Rt	turbulent Reynolds number
$\mathbf{S}_\xi$, $\mathbf{S}_\eta$	diagonalized matrices
T	temperature
t	time
u, v	velocity component in the x- and y-direction respectively
x, y	physical co-ordinates
β', β''	stretching parameter of grid generation in the x- and y-direction respectively
γ	specific heat ratio of gas
δW	implicit boundary condition
ε	turbulent energy dissipation rate
λ	bulk viscosity
μ	viscosity
ξ, η	computational co-ordinates
ρ	density
τ	shear stress

REFERENCES

1. M. K. Looney and J. J. Walsh, 'Mean-flow and turbulent characteristics of free and impinging jet flow', *J. Fluid Mech.*, **147,** 397–429 (1984).
2. M. Wolfshtein, 'Some solutions of the plane turbulent impinging jet', *J. Basic Eng., Trans. ASME*, **92D,** 915–922 (1970).
3. W. W. Bower and D. R. Kotansky, 'A Navier–Stokes analysis of the two-dimensional ground effects problem', *AIAA Paper 76–621*, Palo Alto, CA, 1976.
4. D. R. Kotansky and W. W. Bower, 'A basic study of the VTOL ground effect problem for planar flow', *J. Aircraft*, **15,** 214–221 (1978).
5. M. J. Siclari, D. Migdal and J. L. Palcza, 'The development of theoretical models for jet-induced effects on V/STOL aircraft', *J. Aircraft*, **13,** 938–944 (1976).
6. M. J. Siclari, W. G. Hill Jr. and R. C. Jenkins, 'Investigation of stagnation line and upwash formation', *AIAA Paper 77–615*, Palo Alto, CA 1977.
7. W. W. Bower, R. K. Agarwal and G. R. Peters, 'A theoretical study of two and three dimensional impinging jets', *MERL 79-22*, 1979.
8. A. Rubel, 'Computations of jet impingement on a flat surface', *AIAA J.*, **18,** 168–175 (1980).
9. R. K. Agarwal and W. W. Bower, 'Navier–Stokes computations of turbulent compressible two-dimensional impinging jet flowfields', *AIAA J.*, **20,** 577–584 (1982).
10. R. W. MacCormack, 'The effect of viscosity in hypervelocity impact cratering', *AIAA Paper 69–354*, 1969.
11. R. W. MacCormack, 'Computational efficiency achieved by time splitting of finite difference operators', *AIAA Paper 72–154*, 1972.
12. R. M. Beam and R. F. Warming, 'An implicit factored scheme for the compressible Navier–Stokes equations', *AIAA J.*, **16,** 393–402 (1978).
13. T. H. Pulliam and J. L. Steger, 'On implicit finite difference simulations of three dimensional flows', *AIAA Paper 78–10*, 1978.
14. C. J. Hwang and J. L. Liu, 'Numerical study of two-dimensional impinging jet flowfields', *Proc. 4th Natl Conf. on Mechanical Engineering CSME*, 1987, *pp.* 41–49.
15. R. W. MacCormack, 'A numerical method for solving the equations of compressible viscous flow', *AIAA Paper 81-0110*, 1981.
16. E. von Lavante and W. T. Thompkins Jr., 'An implicit bidiagonal numerical method for solving the Navier–Stokes equations', *AIAA J.*, **21,** 828–833 (1983).
17. D. A. Anderson, J. C. Tannehill and R. H. Pletcher, *Computation Fluid Mechanics and Heat Transfer*, McGraw-Hill, New York, 1984.
18. C. K. G. Lam and K. Bremhorst, 'A modified form of the K–ε model for predicting wall turbulence' *J. Fluids Eng., Trans. ASME*, **103,** 456–460 (1981).
19. V. C. Patel, W. Rodi and G. Scheuerer, 'Turbulence Models for near-wall and low Reynolds number flows: a review', *AIAA J.*, **23,** 1308–1319 (1985).
20. Y. Negano and M. Hishida, 'Improved form of the K–ε model for wall turbulent shear flows', *J. Fluids Eng., Trans. ASME*, **109,** 156–160 (1987).
21. W. T. Thompkins and R. H. Bush, 'Boundary treatments for implicit solutions to Euler and Navier–Stokes equations', *J. Comput. Phys.*, **48,** 302–311 (1982).

22. D. H. Rudy and J. C. Stikwerda, 'Boundary conditions for subsonic compressible Navier–Stokes calculation', *Comput. Fluids*, **9**, 327–338 (1984).
23. H. C. Yee, R. M. Beam and R. F. Warming, 'Boundary approximations for implicit schemes for one-dimensional inviscid equations of gasdynamics', *AIAA J.*, **20**, 1203–1211 (1982).
24. F. B. Hsiao and S. H. Chuang, 'A study of the reversed flow separation of the jet impingement on a varying angle plate', *NSC (R.O.C.) Report, Contract No. CS76-0210-D006-05*, 1988.
25. W. G. Cartwright and P. J. Russell, 'Characteristics of a turbulent slot jet impinging on a plane surface', *Thermodynamics and Fluid Mechanics Conv. 32*, Institute of Mechanical Engineers, Bristol, 1968.
26. J. J. Schauer and R. H. Eustis, 'The flow development and heat transfer characteristics of plane turbulent impinging jets', *Report TR3*, Department of Mechanical Engineering, Stanford University, 1963.